Brillouin Distributed Optical Fiber Sensor Based on a Closed-Loop Configuration

Zhisheng Yang, *Member, OSA*, Marcelo A. Soto, *Member, OSA*, Desmond M. Chow, *Student Member, OSA*, Pabitro Ray, and Luc Thévenaz, *Fellow, IEEE, Fellow, OSA*

(Highly-Scored Paper)

***Abstract*—A Brillouin optical time-domain analysis (BOTDA) method based on a closed-loop control system is proposed to track fast variations of the Brillouin frequency shift along the sensing fiber. While the method eliminates the gain spectral scanning, the exact distributed Brillouin frequency profile is retrieved directly from the output of a closed-loop controller with no need of postprocessing. Moreover, as the operating frequency is being continuously updated to follow the Brillouin frequency change, an unlimited temperature or strain measurement range can be achieved. Both theoretical analysis and experimental results validate that the closed-loop-controlled BOTDA acts as a low-pass filter that considerably rejects the noise from photodetector, with an efficiency that fundamentally outperforms basic averaging. By optimizing the closed-loop parameters, the measurement time is reduced from a few minutes to a couple of seconds compared with standard BOTDA, i.e., two orders of magnitude improvement in terms of measurement speed, while keeping the same accuracy and measurement conditions. If the sampling time interval that is limited by our instrument can be further reduced, the method offers the potentiality of km-range sensing with sub-second measurement time, with an unmatched favorable tradeoff between measurand accuracy and closed-loop delay.**

***Index Terms*—Brillouin scattering, distributed optical fiber sensors, optical fibers, strain and temperature measurements.**

I. Introduction

BRILLOUIN optical time-domain analysis (BOTDA) has been steadily developing over the past three decades, as it offers the capability to monitor temperature and strain distributions over long spans of optical fiber [1], [2]. In a classical BOTDA scheme, a pulsed pump wave interacts with a continuous counter-propagating probe wave through stimulated Brillouin scattering (SBS) when the pump-probe frequency offset falls within the local Brillouin gain spectrum (BGS) of the sensing fiber. By sequentially scanning this pump-probe frequency offset, the Lorentzian-shaped BGS at each fiber position can be reconstructed, and the Brillouin frequency shift (BFS) profile along the fiber can be retrieved by performing spectral fitting on each local BGS [3]. Considering the time-of-flight in the sensing fiber, along with the scan of a large number of frequencies (covering at least the full-width at half-maximum of the BGS) and the use of a large enough number of averaging (to reach a given target measurand accuracy through noise reduction), the whole measurement time turns out to be typically in the order of several minutes, thus restricting classical BOTDA to quasi-static measurements [2]. In order to expedite the measurement process, different methods have been proposed in the literature [4]–[15], in some cases even enabling the use of BOTDA sensing for distributed dynamic measurements. One of these methods circumvents the slow frequency switching time required during scanning, primarily by pre-loading the full set of scanned pump-probe frequency offsets in an arbitrary waveform generator (AWG), commonly designated as fast BOTDA (F-BOTDA) technique [4], [5]. Another way to do without the lengthy frequency scan is to exploit optical frequency combs: the BGS information can be retrieved by generating multi-pump and multi-probe tones simultaneously in a sweep-free BOTDA (SF-BOTDA) technique [6], or utilizing advanced algorithm based on orthogonal frequency division multiplexing (OFDM) [7], [8]. Ultra-fast Brillouin distributed sensing can be realized by reducing the scan to its merest expression using a single probe frequency, as demonstrated in the slope-assisted BOTDA (SA-BOTDA) technique [9]–[11]. This approach presets a fixed pump-probe frequency detuning on one of the lateral slope of the BGS (i.e., detuned from its peak frequency, typically at $\pm\Delta\nu_B/2$), and fast BFS variations on the fiber are directly converted into intensity changes, as a result of local Brillouin gain changes. Based on the working principle of SA-BOTDA, several techniques have been proposed to extend the covered BFS range [12]–[15]. However, the reduction of the BOTDA measurement time using the above-mentioned techniques turns out to systematically degrade other specifications, like a poorer spatial resolution [7], [8], a larger BFS uncertainty [4]–[15], or a limited temperature/strain measurement range [9]–[15].

In this paper, instead of retrieving the information using an open-loop protocol based on the direct response, we propose a novel BOTDA technique based on a closed-loop control (CC-BOTDA) for tracking the BFS evolution at each position along the sensing fiber. Using this totally disruptive approach, the BFS

Manuscript received October 23, 2017; revised December 14, 2017 and December 18, 2017; accepted December 18, 2017. Date of publication December 20, 2017; date of current version March 1, 2018. This work was supported by the Swiss Commission for Technology and Innovation (Project 18337.2 PFNM-NM). *(Corresponding author: Zhisheng Yang.)*

The authors are with the Institute of Electrical Engineering, Swiss Federal Institute of Technology of Lausanne, Lausanne CH 1015, Switzerland (e-mail: zhisheng.yang@epfl.ch; marcelo.soto@epfl.ch; desmond.chow@epfl.ch; pabitro.ray@epfl.ch; luc.thevenaz@epfl.ch).

Color versions of one or more of the figures in this paper are available online at http://ieeexplore.ieee.org.

Digital Object Identifier 10.1109/JLT.2017.2786084

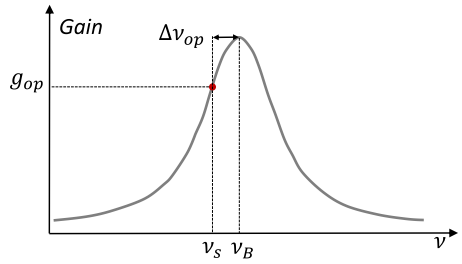

Fig. 1. Operation point of the closed-loop system.

profile can be directly obtained from the output of a closed-loop controller, thereby eliminating the need of frequency scanning and post-processing (i.e., with no spectral fitting involved). The proposed method offers the viability to track fully distributed temperature/strain changes in seconds time-scale, whilst providing a measurand resolution similar or even better than conventional BOTDA. Although this technique requires a single frequency interrogation within the BGS, there is no fundamental limitation to the amount of BFS spectral shift that can be measured, thus enabling the detection of spectral shifts lying far beyond the BGS width. Results demonstrate distributed sensing along a ~10 km-long fiber, with 2 m spatial resolution, using a measurement time of 1.7 s (limited by our instrumentation) and reaching a BFS uncertainty of 0.23 MHz with 256× single-trace averaging. The measurement speed and BFS precision can be easily adjusted by properly setting the parameters of the closed-loop controller. Although, in this paper, the principle of the proposed technique is theoretically described and experimentally demonstrated with a proportional-integral (PI) controller, the concept can be implemented using any suitable closed-loop controller.

II. Working Principle

In classical BOTDA-based sensing, the BGS distribution measured at each fiber position is essentially given by the convolution between the natural Lorentzian-shaped BGS and the pump pulse spectrum [16]. However, for the sake of simplicity and without significant loss of generality, the principle of the proposed CC-BOTDA technique is here described by considering a Lorentzian distribution of arbitrary linewidth given by:

$$g\left(\Delta\nu\right) = \frac{g_B \Delta\nu_B^2}{\Delta\nu_B^2 + 4\Delta\nu^2} \tag{1}$$

where g_B is the Brillouin gain coefficient, $\Delta\nu_B$ is the full width at half maximum (FWHM), and $\Delta\nu = \nu_B - \nu_s$ is the frequency detuning of the pump-probe frequency difference ν_s with respect to the central gain value ν_B (BFS). In the proposed CC-BOTDA, a voluntary detuning is first set at $\Delta\nu = \Delta\nu_{op}$, which further determines an operating pump-probe frequency offset $\nu_s = \nu_B - \Delta\nu_{op}$ and a corresponding gain amplitude g_{op} ($\Delta\nu_{op}$) that can be calculated from (1), as depicted in Fig. 1. When either temperature or strain changes at a given fiber position, the local BGS shifts, hence leading to a different gain amplitude measured at the operating frequency offset ν_s. The key concept behind this approach is to exploit a closed-loop (feedback) control system, for instance a proportional-integral-derivative (PID) controller, in order to track local BGS shifts by compensating the local gain changes through a modified ν_s. This way the predefined reference frequency detuning $\Delta\nu_{op}$ and reference gain amplitude g_{op} are tracked. Adding $\Delta\nu_{op}$ to the current ν_s (set by the controller) gives directly the current BFS at the corresponding fiber position. Note that if the tracking speed is fast enough compared to the dynamics of the spectral shift determined by temperature and strain variations, the pump-probe frequency offset ν_s can be dynamically updated to follow the BGS shift, hence the BFS measurement range is not limited to the linear region of the BGS lateral slope.

In order to achieve the smallest estimated BFS uncertainty and the highest temperature/strain sensitivity, the operating frequency within the BGS should be spectrally located at the point of maximum slope. The mathematical expression of the BGS slope η as a function of detuning $\Delta\nu$ can be represented by the first-order derivative of the BGS distribution described by equation (1)

$$\eta\left(\Delta\nu\right) = \frac{dg}{d\Delta\nu} = \frac{-8g_B\Delta\nu_B^2\Delta\nu}{\left(\Delta\nu_B^2 + 4\Delta\nu^2\right)^2} \tag{2}$$

The frequency detuning $\Delta\nu$ that maximizes the slope $\eta(\Delta\nu)$ can be obtained by equating the second-order derivative of the BGS in equation (1) to zero. This can be expressed as:

$$\frac{d^2g}{d\Delta\nu^2} = \frac{-8g_B\Delta\nu_B^2\left(\Delta\nu_B^2 - 12\Delta\nu^2\right)}{\left(\Delta\nu_B^2 + 4\Delta\nu^2\right)^3} = 0 \tag{3}$$

Solving (3) for $\Delta\nu$ leads to the optimum frequency detuning in CC-BOTDA, corresponding to $\Delta\nu_{op} = \pm\Delta\nu_B/\sqrt{12}$ (e.g., equal to 17.3 MHz for 2 m spatial resolution that corresponds to 60 MHz FWHM of BGS). Note that, incidentally, this optimal frequency detuning is also the optimal one for schemes like SA-BOTDA [10]. However, SA-BOTDA is an open loop system that requires the operating spectral range must be large enough, this normally prevents the system from operating at this optimal point, but positioned in the central region of the lateral slope ($\Delta\nu_{op} = \pm\Delta\nu_B/2$) [10]. With respect to the optimal operating point, this compromise leads to a signal-to-noise ratio (SNR) penalty as analyzed in Appendix B. It is important to mention that the real BGS shape (resulting from the convolution of the pump pulse spectrum and the natural BGS shape) may differ from a perfect Lorentzian shape, as reported in [16]. Rigorously the position of the ideal operation point $\Delta\nu_{op} = \pm\Delta\nu_B/\sqrt{12}$ needs to be recalculated, particularly for short pulses, but the inherent robustness of a closed-loop system to slight deviations and nonlinearities makes such an offset not at all critical.

Since the BFS distribution over the sensing fiber has to be assumed non-uniform in real situations, the implementation of the CC-BOTDA technique considers the sensing fiber (of length L) as a concatenation of N short fiber segments of identical length ($N = L/\Delta z$, with Δz the spatial resolution of the sensor) [10], as shown in Fig. 2. The technique preferably requires that a reference BFS is initially measured in each fiber segment $\nu_B(z)$ using a standard BOTDA interrogation. The probe wave is then temporally segmented in N slots of identical duration

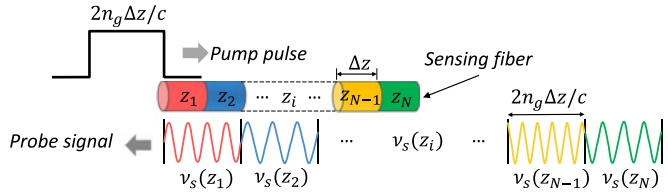

Fig. 2. Schematic of the proposed method tailoring the probe frequency.

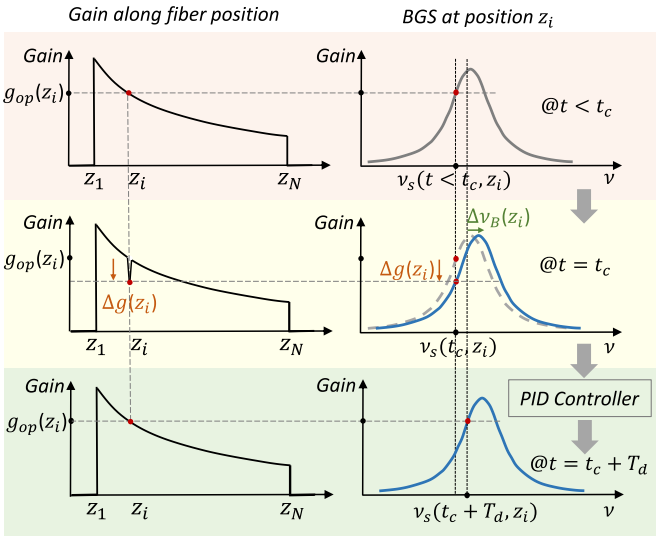

Fig. 3. CC-BOTDA working principle.

$(2n_g\Delta z/c$, where c/n_g is the group velocity). The pump-probe frequency offset $\nu_s(z)$ in each time slot is set to the reference BFS profile $\nu_B(z)$ subtracting (or adding) the preset detuning $\Delta\nu_{op}$. When the pump pulse arrives at a given fiber position z_i, it will interact with the corresponding probe frequency matching the expected detuning $\Delta\nu_{op}$ thereby giving the reference gain amplitude $g_{op}(z_i)$.

Note that in a calibrated CC-BOTDA system and under steady-state conditions, the probe is expected to be exactly detuned from the local BFS by $\Delta\nu_{op}$ at any fiber position. In such a case, as shown in the upper-left frame of Fig. 3, the captured BOTDA trace exhibits a uniform exponential decay due to the pump attenuation, independently of the actual BFS profile. If, at time t_c the local BGS shifts due to an external perturbation (see central frame in Fig. 3), a corresponding local gain change $\Delta g(z_i)$ is induced with respect to the reference value $g_{op}(z_i)$. The principle of the proposed CC-BOTDA is based on using a closed-loop control system that compares the measured gain offset (with respect to the operating point) with the reference gain and feeds back an adjusted probe frequency $\nu_s(z_i)$ into the corresponding time slot z_i. The probe frequency is then sequentially adjusted until the current gain matches the reference gain, thereby enabling the system to gradually return to the operating point as shown in the bottom frame of Fig. 3. An essential parameter of the closed-loop controller is the number of tracking steps n required to return to the operating point. This number of tracking steps and the time period T_s for each tracking step (i.e., sampling interval between consecutive measurements) define

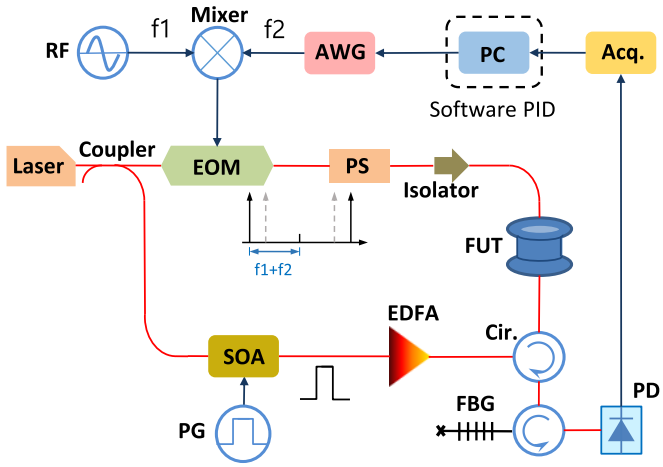

Fig. 4. Experimental setup.

the total time T_d needed to reach the steady-state value, which can be expressed as:

$$T_d = nT_s \tag{4}$$

This time T_d actually determines the speed of the tracking system. Note that in contrast to existing BOTDA schemes, in this case the BFS profile is not obtained by the usual BGS spectral fitting (as in standard BOTDA) or by direct conversion of gain amplitude variations (as in SA-BOTDA), but is retrieved directly from the controller output $\nu_s(t_c + T_d, z_i) \pm \Delta\nu_{op}$, thereby enabling dynamic measurement of external perturbations.

III. Experimental Setup

The experimental setup implemented to validate the proposed method is shown in Fig. 4. Pump and probe branches are created from a distributed feedback laser (DFB) using an optical splitter. In the pump branch the continuous-wave light is intensity-modulated with high extinction ratio (>50 dB) to a 20 ns optical pulse (which corresponds to 2 m spatial resolution) using a semiconductor optical amplifier (SOA) driven by an electrical pulse generator. The pulse is then amplified using an erbium-doped fiber amplifier (EDFA) and launched into a ∼9.3 km-long sensing fiber through a circulator. In the probe branch, a carrier-suppressed double-sideband (CS-DSB) wave is generated using an electro-optic modulator (EOM) having a high extinction ratio (40 dB) and operating at the null transmission point. The driving electrical signal consists of 4650 time-domain slots (number defined by the ratio between the fiber length and the spatial resolution), and the frequency in each slot is set to match the corresponding initial local BFS (around 10.46 GHz) minus $\Delta\nu_{op}$ (17. 3 MHz). Due to the limited bandwidth (2 GHz) of our arbitrary waveform generator (AWG), the high-frequency modulated electrical signal (around 10.44 GHz) is generated by mixing a microwave signal at the constant frequency $f_1 = 10.2$ GHz with the variable low-frequency signal at $f_2 = 150$–300 MHz generated by the AWG. Note that in such a configuration there are actually two frequency components (at $f_1 - f_2$ and $f_1 + f_2$) existing in the mixed signal, out of which

only the frequency component $f_1 + f_2$ actually experiences the narrow band Brillouin interaction. To minimize the polarization fading effect, the modulated probe wave is sent to a polarization switch and then launched to the sensing fiber through an isolator. After experiencing the SBS interaction with the pump pulse in the sensing fiber, the lower-frequency probe sideband is selected using a fiber Bragg grating (FBG) with 6 GHz bandwidth and then detected by a 75 MHz bandwidth photodetector (PD).

Note that although the derivative (D) term in a PID controller can predict system behavior and thus help reducing the overshoots and oscillations imposed by the integral (I) term, it would also magnify the impact of noise, which is not recommended since the SNR level is considered as one of the most critical sensing performance in our system. Therefore, as a proof-of-concept, a software-based PI controller is implemented, thus directly linking the acquired local gain values and PI outputs to update the probe frequency into the AWG. Due to the 256× time-averaging and the time required for the AWG to upload all frequency values in each tracking cycle, the sampling interval for the feedback loop (i.e., the tracking step interval) amounts to ∼1.7 s, which is essentially limited by the non-optimum slow data transfer speed of our AWG. By recording the probe frequencies for each tracking step, the BFS evolution as a function of time is obtained for all fiber positions.

Note that one of the potential drawbacks of the proposed CC-BOTDA is that the technique can be affected by pump power fluctuations due to the laser source or to spatially-dependent losses that occur in dynamic scenarios. While laser power fluctuation could be eventually monitored and compensated, the losses originating from time-varying stresses could bias the estimation of the BFS along the fiber, similarly to any other method in which BFS variations are converted into intensity variations.

IV. Experimental Results and Discussion

The initial step of the process is to determine the initial BFS profile along the entire sensing fiber using standard BOTDA interrogation. In our experiments, the BGS along the fiber has been measured 20 consecutive times using a conventional full-scanning method with 1 MHz scanning step and 256 averages per trace. The mean value obtained from the BFS profiles has been used as a reference, which has an uncertainty of 0.24 MHz (defined by the standard deviation) at the end of the sensing fiber. From this reference BFS profile, the operating frequency within the BGS has been defined, while the frequency values associated to the different fiber segments are uploaded into the AWG.

After the calibration process, the proportional (K_P) and integral (K_I) PI coefficients are optimized by monitoring the closed-loop impulse response of the system by applying an instantaneous (sharp) temperature step to a 6 m-long fiber section. With an initial reference BFS profile measured at 22 °C, and activating the tracking system when the hotspot section is at 32 °C, the response to an equivalent temperature step of 10 °C is measured. Following a standard procedure for the adjustment of a PI controller, K_P is firstly adjusted while K_I is set to zero ($K_I = 0$). The response of the PI output is shown in Fig. 5. It is

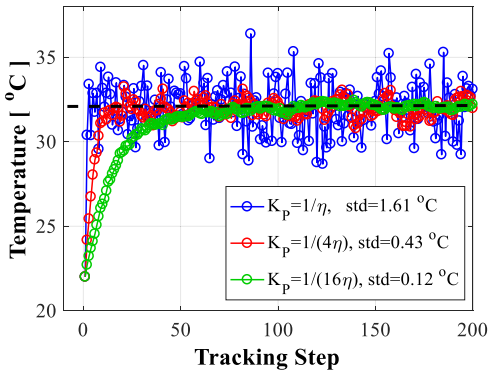

Fig. 5. Output of the tracking system for a 10 °C temperature step using only a proportional term with coefficient K_P.

observed that, when K_P is set to the inverse of the BGS slope at the operation point ($K_P = 1/\eta$), the feedback loop can follow the 10 °C temperature change in one tracking step (∼1.7 s), as shown by the blue curve in Fig. 5. However, this fast response leads to a relatively large temperature uncertainty (1.61 °C) at the steady-state, which is calculated as 7 times worse than the result obtained using classical BOTDA scanning (∼0.24 °C). Note that the frequency uncertainty can be greatly reduced by reducing the value of K_P, at the expense of a few more tracking steps. As exemplified by the green curve in Fig. 5, the uncertainty can be significantly reduced by a factor 13 using 45 tracking steps. This feature indeed highlights one of the biggest advantage of the proposed tracking-based CC-BOTDA method, i.e., a linear relationship between the number of repeated measurements—here the tracking steps—and the noise reduction. This has to be compared with a standard BOTDA where noise reduction is obtained by averaging and thus follows a square-root dependence on the number of repeated measurements, so that a much larger number of averaged traces ($13^2 = 169$ times more) is required to reach the same uncertainty.

In order to explicitly explain the experimentally observed dynamics in CC-BOTDA, a theoretical model has been built using a discrete-time analysis based on z-domain transformation (see Appendix), in which the step response of the system in the discrete time domain is derived as:

$$r[n] = 1 - (1 - K)^n \tag{5}$$

where $K = \eta K_P$. Equation (5) points out that when $K = 1$ (i.e., $K_P = 1/\eta$), the system can reach the steady state value by using only one tracking step, as experimentally validated in Fig. 5. Furthermore, Fig. 6 shows the step response obtained from equation (5) for three different values of K (same parameters as those used in Fig. 5). A comparison between Figs. 5 and 6 shows a good agreement between experimental and theoretical results, thus further validating the theoretical analysis as well as the experimental results.

In the case of $K < 1$, the number of the required tracking steps is derived as:

$$n = \frac{\log(1 - d)}{\log(1 - K)} \tag{6}$$

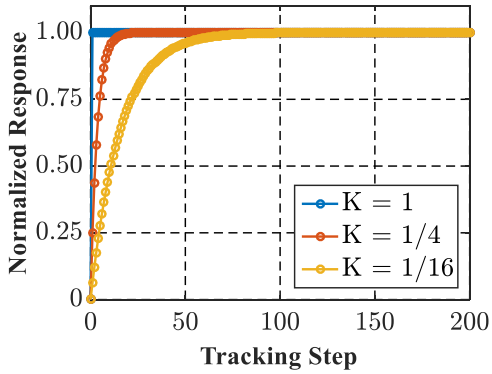

Fig. 6. Theoretical calculation of system response versus tracking steps with unit step function input.

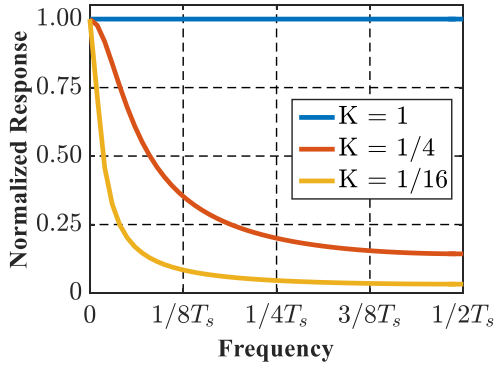

Fig. 8. The spectral response of the tracking system obtained from (7) for different K values.

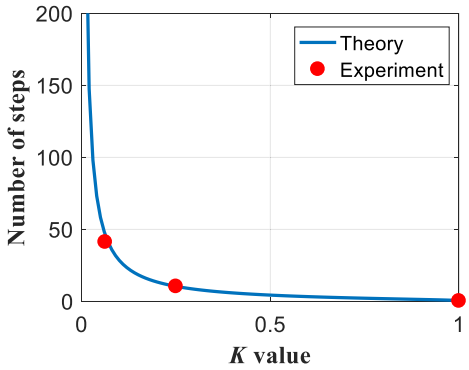

Fig. 7. The calculated number of tracking steps needed to attain 0.95 of steady state response level by changing K value settings.

where d is the target level of system response to be considered as steady state. When d is reasonably set as 0.95, the required number of tracking steps can be calculated as a function of K, as shown in Fig. 7, which is in good agreement with the experimental results (red dots).

In order to explore the noise reduction feature when reducing the value of K, the spectral response of the system is analyzed (see Appendix A), resulting in a spectral-domain transfer function given as:

$$|T(j\omega)| = \frac{K}{\sqrt{K^2 + 2(1-K)[1-\cos(\omega T_s)]}} \tag{7}$$

Note that in the case of $K = 1$, $|T(j\omega)|$ becomes equal to 1, which means that the entire signal and noise from the photodetector are transferred to the CC-BOTDA system, as explained in details in Appendix A. As analyzed before, in this case the system only uses one tracking step reaching steady state with no contribution from feedback loop, showing a great similarity to the SA-BOTDA method that directly converts the gain variation to BFS change. In other words, this is equivalent to acquire a single Brillouin gain trace using standard BOTDA, while the lack of frequency scanning and post-processing results in poorer SNR performance with respect to standard BOTDA, given by a factor derived in Appendix B:

$$\frac{\sigma_\nu^{\text{max\_slope}}}{\sigma_\nu^{\text{standard}}} = \frac{8}{9}\sqrt{N} \tag{8}$$

where N is the number of frequency scanning steps within FWHM of the BGS used by the standard BOTDA technique. The factor expressed by equation (8) is calculated as ~7 using 1 MHz frequency increment in the case of 2 m spatial resolution that corresponds to 60 MHz FWHM of BGS. This is in full agreement with the BFS uncertainty of blue curve shown in Fig. 5. According to the square law dependence between SNR and averages time, this 7 times SNR degradation in CC-BOTDA can be compensated by costing 49 times more trace averaging, thus reaching the same SNR performance as in standard BOTDA. It indicates that measurements with similar SNR performance can be acquired inherently faster with CC-BOTDA than standard BOTDA, as the latter requires at least N times frequency scanning ($N = 60$ in the case of 2 m spatial resolution) to reconstruct the BGS for post-processing. Note that practically the spectral scanning range for standard BOTDA is a few hundreds of MHz, which is far larger than FWHM of BGS, making the BFS retrieving process even slower.

Moreover, in the case of $K < 1$, the spectral behavior described by (7) turns out to depend only on the term $[1 - \cos(\omega T_s)]$, for a given value of K. Note that according to the Nyquist sampling theorem, the maximum signal bandwidth of the system is ultimately limited to $f_{\max} = 1/(2T_s)$, hence the valid range of the variable ωT_s in (7) can only span from 0 to π. As a consequence, the value of the term $[1 - \cos(\omega T_s)]$ increases as the value of ωT_s gets larger, indicating that in this case $|T(j\omega)|$ exhibits a discrete low-pass filter property. This low pass filtering effect improves the overall noise performance of the CC-BOTDA system. The spectral shape of this low-pass filter is determined by the value of K, as illustrated in Fig. 8.

Since the spectral density of the noise from the photodetector is constant, the area under the curve in Fig. 8 scales the relative noise for the respective K values, which could be calculated by integrating equation (7) over ω within the Nyquist sampling window. The theoretical noise reduction factor in linear scale as a function of K is shown in Fig. 9 (blue line), which also shows experimental results obtained from the traces in Fig. 5,

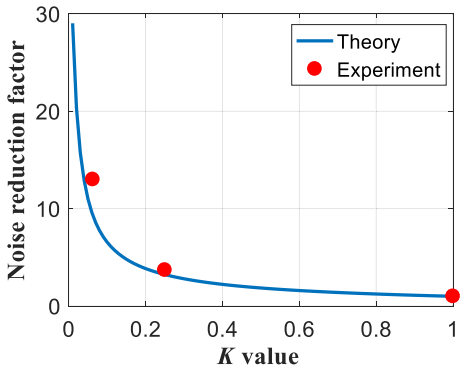

Fig. 9. The change of noise reduction factor in linear scale by varying K parameter. Experimental results (steady state std from Fig. 5) are indicated in red.

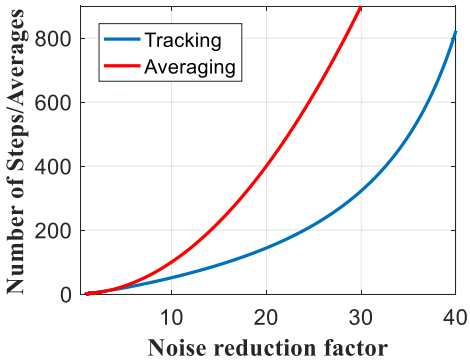

Fig. 10. The required averages or tracking steps versus noise reduction factor in linear scale between the tracking system and average method used in standard BOTDA system.

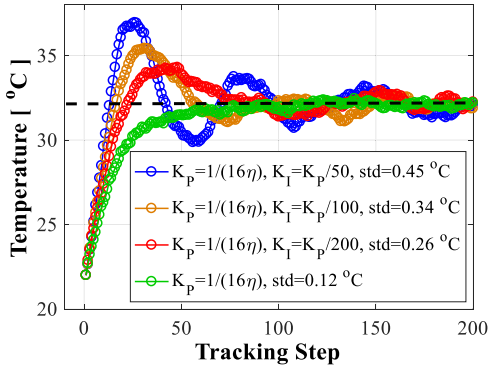

Fig. 11. PI controller with constant K = 1/16 but different K_I.

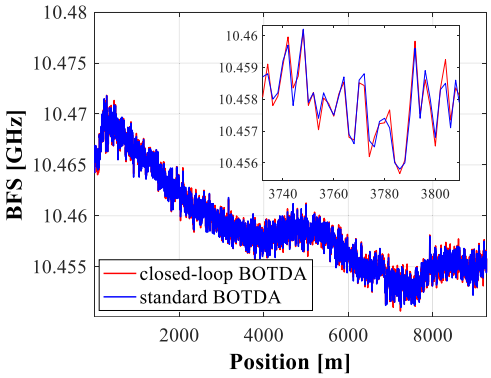

Fig. 12. BFS profiles measured using CC-BOTDA and standard BOTDA with 256 averaging times. The parameters in CC-BOTDA are set as $K_P = 1/(16\eta)$ and $K_I = K_P/200$.

and also indicating a good agreement between the experimental and theoretical results. This analysis indicates that the poor SNR performance when $K = 1$ given by equation (8) can be greatly improved by reducing the value of *K*, and since both the noise reduction factor and the number of tracking steps exclusively depend on the value of K, the relation between these two parameters can be obtained by mapping Fig. 9 into Fig. 7, as shown by the blue curve in Fig. 10, which reveals as a quasi-linear function before the noise reduction factor (in linear scale) reaches 20. This figure also shows (see red line) the number of averages required for achieving a desired noise reduction factor (parabolic curve), thus highlighting the reduced number of acquisitions required by the CC-BOTDA as compared to standard BOTDA methods. Note that the tracking sampling interval in our system is limited by the AWG data uploading (1.7 seconds) and each Brillouin gain trace averaging lies in milliseconds time-scale. Therefore, keeping K = 1 and using a large number of trace averages may still be a preferable solution to achieve highest tracking speed and the best SNR performance. Nevertheless, the value of T_s does not affect the number of tracking steps as well as the noise reduction factor, since both are related only to *K*. Hence, if T_s is reduced and made comparable to the trace averaging time, a low *K* value combined with a certain number of averages can offer a better performance for CC-BOTDA.

In addition, the tracking time of our CC-BOTDA system can be further reduced using an integrator (K_I) in conjunction with a low K_P value thereby also maintaining a low noise level, as shown in Fig. 11. The larger the value of K_I, the higher are the overshoot and oscillations, thus increasing the temperature uncertainty of the measurement within the transient time. It can be observed that $K_I = K_P/200$ is an appropriate choice to reach the same level of uncertainty as obtained with the classical BOTDA interrogation, defining a temperature uncertainty of 0.26 °C at ∼9.3 km distance (being ∼0.24 °C for classical BOTDA). To compare both the techniques, Fig. 12 shows the distributed BFS profile measured along the entire sensing fiber using the proposed CC-BOTDA system (red curve) and standard BOTDA (blue curve) with the same number of averages (256×). A good matching between the two curves is observed, including the longitudinal BFS oscillations induced by the fiber coiling, as shown in Fig. 12 inset.

Finally, in order to verify the tracking ability of the proposed CC-BOTDA system over a large measurable BFS range, the temperature of the hotspot fiber section has been gradually increased from 22 °C up to 53 °C, with a rate of 0.08 °C/s (i.e., 0.14 °C per tracking step). Results obtained using different combinations of K_P and K_I are shown in Fig. 13, where the blue curves represent the reference temperature evolution measured by a high-resolution electronic thermometer. It confirms that the system can follow the temperature evolution in quasi-real time using $K_P = 1/\eta$, but with relatively large temperature uncertainty. As K_P is reduced, the temperature uncertainty decreases linearly, but at the cost of introducing a small delay. As shown

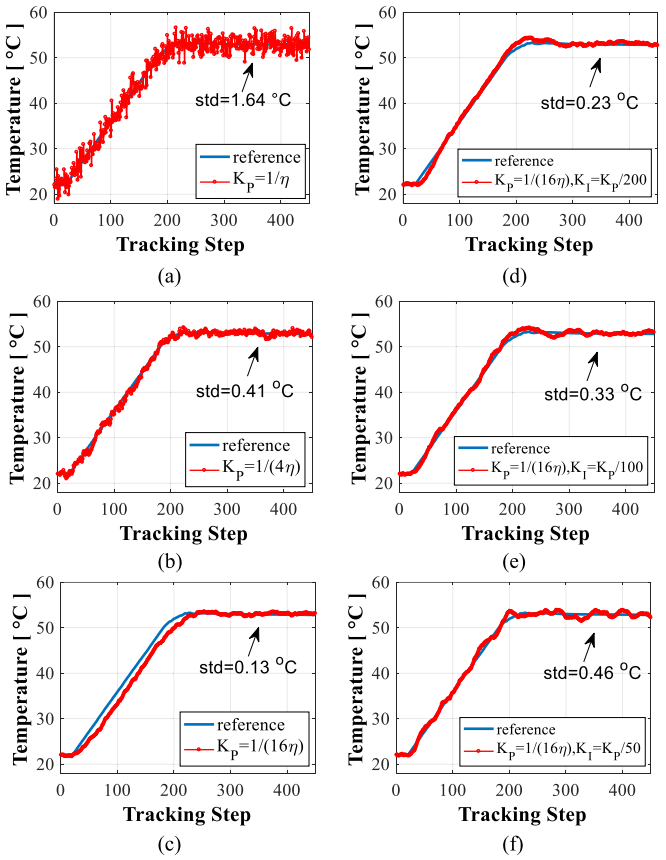

Fig. 13. Output of PI tracking system when applying a gradual temperature change at the rate of 0.08 °C/s, using different K_P and K_I coefficients.

in Fig. 13(c), when $K_P = 1/(16\eta)$, the delay turns out to be ∼15 steps (i.e., ∼25 s), while the temperature uncertainty is 2-fold better than standard BOTDA (which typically needs a few hundred scanning steps) with similar averaging. By introducing the integral term K_I with a low K_P value, the tracking speed can be increased, as shown in Fig. 13(d)–(f). A negligible delay (tracking in about one step, i.e., ∼1.7 s) could be observed when setting $K_I = K_P/100$ or $K_I = K_P/50$, leading to a temperature uncertainty similar to a classical BOTDA that however takes a few minutes to finish one BFS retrieving process (including spectral scanning and post-processing). Among them the best overall performance in terms of both tracking speed and temperature accuracy is found to be in the case illustrated in Fig. 13(d), where the integral term plays an important role to accelerate the tracking speed. This actually demonstrates that the CC-BOTDA can reduce the measurement time by two orders of magnitude with no penalty on the measurand accuracy. It must be highlighted that the precise tracking of the temperature over the entire 31 °C range also confirms that the method has an unlimited measurand range, which is not restricted to the BGS width.

V. Conclusion

A novel CC-BOTDA method is proposed to provide fast distributed temperature/strain sensing by optimally revisiting the procedure for collecting the relevant information utilizing a software PI controller, which offers several advantages with respect to standard BOTDA: 1) Only one operating probe frequency is interrogated, which totally suppresses the necessity of a spectral scanning process that often contains redundant information; 2) At each tracking step the operating frequency is updated to follow the shift of BGS, thus enabling unlimited BFS measurement range that is far beyond the BGS width; 3) The amount of BFS change can be directly obtained from the PI controller output, without additional post-processing.

Both the analytical z-domain model and the experimental results demonstrate that with respect to standard BOTDA, by solely setting the proportional coefficient (K_P) as the inverse of the BGS slope at operating point ($1/\eta$), while disabling the contribution of integral coefficient (K_I), the CC-BOTDA system possesses a fundamental advantage that costs a lesser total measurement time to reach a target SNR compared with standard BOTDA with frequency scanning. Moreover, by further reducing K_P value while keeping $K_I = 0$, the system exhibits a low-pass filter property, which leads to less expense of additional tracking steps compared with using trace averages to reach the same SNR. However, the data re-uploading time of our AWG (T_s = 1.7 s), which is far longer than the time for single trace averaging (in ms time-scale), makes such a benefit only obtained for large noise reduction, regarding the squared growth of the number of averaging. Note that both the tracking steps and the noise reduction factor are not related to T_s, hence the above mentioned fundamental benefit can be realized by massively reducing T_s using more advanced AWG circuitry, in which the measurement speed would be drastically boosted with no negative impact. Even with our rather slow AWG, by experimentally optimizing both K_P and K_I values, the trade-off between estimated BFS accuracy and measurement time with respect to the case of using K_P only can be greatly alleviated, thus enabling the system to report the temperature profile along the fiber in every 1.7 s with 0.23 °C uncertainty. While for each BFS retrieving process using standard BOTDA with same BFS uncertainty, the time spent for spectral scanning (1 MHz scanning step, 200 MHz scanning range) associated with that for post-processing turns out to be more than 3 minutes, demonstrating that the closed-loop system can reduce the measurement time by two orders of magnitude (from minutes scale to seconds scale), while keeping the same accuracy and measurement conditions.

Appendix A

In this appendix, we present a mathematical analysis for the CC-BOTDA based on a proportional controller (K_P). Here we assume for simplicity that the change in Brillouin frequency for each tracking step lies within the linear region of the slope of the Lorentzian-shaped BGS. Thus, without losing generality, the linear region of the Lorentzian-shaped BGS can be approximated to a first-order linear function. When subjected to an external perturbation, this linear function shifts in frequency, as shown Fig. 14, where ν_s^0 is the initial frequency of operation that results in the reference gain (g_{op}) with b as the y-intercept. Thus, the initial linear function represented as a grey color line

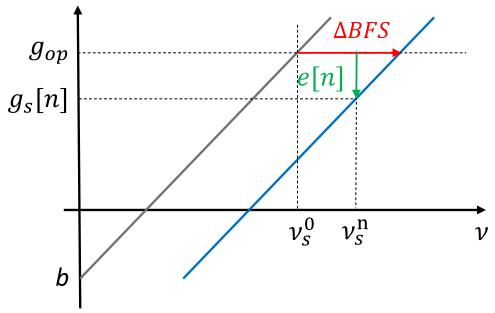

Fig. 14. Schematic representation of frequency shifted linear region of the BGS slope.

in Fig. 14 can be mathematically expressed by equation (1A), where n represents the nth iteration in the closed-loop control and η is the linear slope.

$$g_{op}\left[n\right] = \eta\nu_s^0\left[n\right] + b \tag{1A}$$

A discrete-time differentiation of (1A) gives:

$$g_{op}\left[n\right] - g_{op}\left[n-1\right] = \eta\left(\nu_s^0\left[n\right] - \nu_s^0\left[n-1\right]\right) \tag{2A}$$

Applying z-transform, we may rewrite (2A) in z-domain as:

$$G_{op}\left(z\right) - z^{-1}G_{op}\left(z\right) = \eta\left(N_s^0\left(z\right) - z^{-1}N_s^0\left(z\right)\right) \tag{3A}$$

simplified to:

$$G_{op}\left(z\right) = \eta N_s^0\left(z\right) \tag{4A}$$

Further, the frequency shifted BGS slope shown as a blue line in Fig. 14 can be written as:

$$g_s\left[n\right] = \eta\left(\nu_s\left[n\right] - \Delta BFS\right) + b \tag{5A}$$

where $g_s[n]$ is the measured gain value for an operating frequency of $\nu_s[n]$ at the nth tracking step. Nevertheless, the operating frequency at nth iteration can also be expressed in terms of the initial operating frequency as:

$$\nu_s\left[n\right] = \nu_s^0\left[n\right] + \sum_{m=1}^{n}\Delta\nu_s\left(m\right) \tag{6A}$$

Similar to the previous case, a discrete-time derivative of the linear function (5A) results in:

$$g_s\left[n\right] - g_s\left[n-1\right] = \eta\left(\nu_s\left[n\right] - \nu_s\left[n-1\right]\right) \tag{7A}$$

and subsequently in z-domain can be written as

$$G_s\left(z\right) = \eta N_s\left(z\right) \tag{8A}$$

Combining equations (4A) and (8A) the following transfer function can be obtained:

$$T\left(z\right) = \frac{G_s\left(z\right)}{G_{op}\left(z\right)} = \frac{N_s\left(z\right)}{N_s^0\left(z\right)} \tag{9A}$$

The above equation states that gain and frequency detuning have the same transfer function $T(z)$.

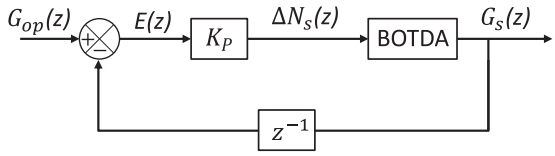

Fig. 15. Diagram of CC-BOTDA working principle in z-domain.

Note that the term $\eta(\nu_s[n] - \nu_s[n-1])$ in (7A) may also be expressed as $\Delta\nu_s[n]$, thereby transforming equation (7A) to:

$$g_s\left[n\right] - g_s\left[n-1\right] = \eta\Delta\nu_s\left[n\right] \tag{10A}$$

which in z-domain corresponds to:

$$\left(1 - z^{-1}\right)G_s\left(z\right) = \eta\Delta N_s\left(z\right) \tag{11A}$$

where $\Delta N_s(z)$ is the required change in the detuning frequency. Following the working diagram of our CC-BOTDA method in z-domain described as Fig. 15, the feedback control error function $E(z)$ as the difference between the reference gain and current gain is expressed as:

$$E\left(z\right) = G_{op}\left(z\right) - z^{-1}G_s\left(z\right) \tag{12A}$$

and $\Delta N_s(z)$ can be derived as:

$$\Delta N_s\left(z\right) = K_P E\left(z\right) = K_P\left(G_{op}\left(z\right) - z^{-1}G_s\left(z\right)\right) \tag{13A}$$

where K_P is the value of proportional constant used in the feedback control. Combining (11A) and (13A), we could further derive the relationship between $G_{op}(z)$ and $G_s(z)$:

$$\left(1 - z^{-1}\right)G_s\left(z\right) = \eta K_P\left(G_{op}\left(z\right) - z^{-1}G_s\left(z\right)\right) \tag{14A}$$

Rearranging (14A), the desired transfer function is given by the relation:

$$T\left(z\right) = \frac{G_s\left(z\right)}{G_{op}\left(z\right)} = \frac{K}{\left(K-1\right)+z} \tag{15A}$$

where $K = \eta K_P$.

From equation (9A), the transfer function in terms of operating frequency can be written as:

$$T\left(z\right) = \frac{N_s\left(z\right)}{N_s^0\left(z\right)} = \frac{K}{\left(K-1\right)+z} \tag{16A}$$

In order to understand the behavior of such a closed-loop feedback control, the unit step response of the system is evaluated by multiplying the system transfer function with the unit-step function $z/(z-1)$:

$$\begin{aligned} R\left(z\right) &= T\left(z\right)\frac{z}{z-1} \\ &= \frac{1}{1-z^{-1}} - \frac{1}{1-\left(1-K\right)z^{-1}} \end{aligned} \tag{17A}$$

An inverse z-transformation yields the discrete-time step response of the system:

$$r\left[n\right] = 1 - \left(1-K\right)^n \tag{18A}$$

It can be observed that when $K = 1$, which means K_P is exactly equal to the inverse of the slope $(1/\eta)$ at BGS operating

point, equation (18A) is independent of the number of iterations thereby allowing the system to reach steady-state in a single step.

In the case of $K < 1$, the number of the required tracking steps are derived as:

$$n = \frac{\log(1-d)}{\log(1-K)} \tag{19A}$$

where d is the target steady-state of system response. In most applications d is typically chosen as 80–95% of the final value.

In order to explore the noise reduction characteristics of our CC-BOTDA system, further analysis is performed in the spectral domain by substituting $z = e^{j\omega T_s}$ in the system transfer function (16A):

$$T(j\omega) = \frac{K}{(K-1) + e^{j\omega T_s}} \tag{20A}$$

The absolute value of the equation is given by:

$$\begin{aligned} |T(j\omega)| &= \sqrt{\frac{K}{(K-1)+e^{j\omega T_s}} \times \frac{K}{(K-1)+e^{-j\omega T_s}}} \\ &= \frac{K}{\sqrt{K^2 + 2(1-K)[1-\cos(\omega T_s)]}} \end{aligned} \tag{21A}$$

As illustrated by equation (21A), $|T(j\omega)|$ is a low-pass filter, highlighting the improved performance of CC-BOTDA in terms of noise rejection. It may be noted that, when K is set to unity, the low-pass filtering effect cease to exist thereby allowing maximum noise level from the photodetector, hereafter defined as σ_g.

APPENDIX B

An uncertainty in the estimated BFS may arise due to the direct conversion of gain change to frequency variation. In order to estimate such an uncertainty, the term $\Delta\nu_{op}$ in (2) is substituted with a detuned operating frequency of $\Delta\nu_{op} = \pm\Delta\nu_B/\sqrt{12}$, and is calculated as:

$$\sigma_\nu^{\max\_slope} = \frac{4\Delta\nu_B}{3\sqrt{3}} \frac{\sigma_g}{g_B} \tag{1B}$$

where $\Delta\nu_B$ is the FWHM of the BGS, and σ_g is the noise level (determining Brillouin gain uncertainty) that is defined in Appendix A. Given the SNR conditions, in a standard BOTDA setup using a full frequency scanning complemented with a quadratic fitting post-processing such an uncertainty is given by the relation [3]:

$$\sigma_\nu^{\text{standard}} = \frac{\sqrt{3}\Delta\nu_B}{2\sqrt{N}} \frac{\sigma_g}{g_B} \tag{2B}$$

where *N* is the number of frequency scanning steps within the FWHM of the BGS. By taking the ratio between equation (1B) and (2B), the BFS uncertainty improvement using a standard BOTDA is obtained as:

$$\frac{\sigma_\nu^{\max\_slope}}{\sigma_\nu^{\text{standard}}} = \frac{8}{9}\sqrt{N} \tag{3B}$$

As an example if $N = 60$ which corresponds to the case of a 2 m spatial resolution (for a 60 MHz FWHM of BGS) and 1 MHz frequency scanning step, the BFS uncertainty using standard BOTDA is calculated as 6.88 times smaller with respect to gain-frequency conversion performed at the operating BGS point using a single frequency probe. It means that the latter case needs ∼49 times more averaging to reach the same performance as in a standard BOTDA. In the sense of supporting larger temperature or strain range within each tracking step, it is better to move the operating point from the largest slope point ($\Delta\nu_{op} = \pm\Delta\nu_B/\sqrt{12}$) to the point at FWHM ($\Delta\nu_{op} = \pm\Delta\nu_B/2$), which is exactly the case in SA-BOTDA [10]. However, in this scenario an even larger uncertainty improvement benefits to the standard BOTDA and is calculated to be $2\sqrt{N}/\sqrt{3}$. In this case, when $N = 60$ it corresponds to 8.9 times improvement, thereby indicating that ∼81 times more averages are required so as to reach the same performance as in standard BOTDA.

REFERENCES

[1] T. Horiguchi, K. Shimizu, T. Kurashima, M. Tateda, and Y. Koyamada, "Development of a distributed sensing technique using Brillouin scattering," *J. Lightw. Technol.*, vol. 13, no. 7, pp. 1296–1302, Aug. 1995.

[2] A. Motil, A. Bergman, and M. Tur, "State of the art of Brillouin fiber-optic distributed sensing," *Opt. Laser Technol.*, vol. 78, pp. 81–103, 2016.

[3] M. A. Soto and L. Thévenaz, "Modeling and evaluating the performance of Brillouin distributed optical fiber sensors," *Opt. Express*, vol. 21, no. 25, pp. 31347–31366, Dec. 2013.

[4] Y. Peled, A. Motil, and M. Tur, "Fast Brillouin optical time domain analysis for dynamic sensing," *Opt. Express*, vol. 20, no. 8, pp. 8584–8591, Mar. 2012.

[5] Y. Dong *et al.*, "High-spatial-resolution fast BOTDA for dynamic strain measurement based on differential double-pulse and second-order sideband of modulation," *IEEE Photon. J.*, vol. 5, no. 3, Jun. 2013, Paper no. 2600407.

[6] A. Voskoboinik, O. F. Yilmaz, A. W. Willner, and M. Tur, "Sweep-free distributed Brillouin time-domain analyzer (SF-BOTDA)," *Opt. Express*, vol. 19, no. 26, pp. B842–B847, Dec. 2011.

[7] J. Fang, P. Xu, Y. Dong, and W. Shieh, "Single-shot distributed Brillouin optical time domain analyzer," *Opt. Express*, vol. 25, no. 13, pp. 15188–15198, Jun. 2017.

[8] C. Zhao *et al.*, "BOTDA using channel estimation with direct-detection optical OFDM technique," *Opt. Express*, vol. 25, no. 11, pp. 12698–12709, May 2017.

[9] R. Bernini, A. Minardo, and L. Zeni, "Dynamic strain measurement in optical fibers by stimulated Brillouin scattering," *Opt. Lett.*, vol. 34, no. 17, pp. 2613–2615, Sep. 2009.

[10] Y. Peled, A. Motil, L. Yaron, and M. Tur, "Slope-assisted fast distributed sensing in optical fibers with arbitrary Brillouin profile," *Opt. Express*, vol. 19, no. 21, pp. 19845–19854, Sep. 2011.

[11] A. Motil, O. Danon, Y. Peled, and M. Tur, "Pump-power-independent double slope-assisted distributed and fast Brillouin fiber-optic sensor," *IEEE Photon. Technol. Lett.*, vol. 26, no. 8, pp. 797–800, Apr. 2014.

[12] J. Urricelqui, A. Zornoza, M. Sagues, and A. Loayssa, "Dynamic BOTDA measurements based on Brillouin phase-shift and RF demodulation," *Opt. Express*, vol. 20, no. 24, pp. 26942–26949, Nov. 2012.

[13] D. Ba *et al.*, "Distributed measurement of dynamic strain based on multi-slope assisted fast BOTDA," *Opt. Express*, vol. 24, no. 9, pp. 9781–9793, Apr. 2016.

[14] D. Zhou *et al.*, "Slope-assisted BOTDA based on vector SBS and frequency-agile technique for wide-strain-range dynamic measurements," *Opt. Express*, vol. 25, no. 3, pp. 1889–1902, 2017.

[15] G. Yang, X. Fan, and Z. He, "Strain dynamic range enlargement of slope-assisted BOTDA by using Brillouin phase-gain ratio," *J. Lightw. Technol.*, vol. 35, no. 20, pp. 4451–4458, Oct. 2017.

[16] M. Alem, M. A. Soto, M. Tur, and L. Thévenaz, "Analytical expression and experimental validation of the Brillouin gain spectral broadening at any sensing spatial resolution," *Proc. SPIE*, vol. 10323, 2017, Paper no. 103239J.

Zhisheng Yang received the B.E. degree in optoelectronics from the Beijing Institute of Technology, Beijing, China, in 2010, and the Ph.D. degree in communication and information system from the Beijing University of Posts and Telecommunications, Beijing, in 2016. His Ph.D. research work, performed at the institute of Information Photonics and Optical Communications, was focused on distributed optical fiber sensors.

In 2016, he joined the Group for Fibre Optics, Swiss Federal Institute of Technology of Lausanne, Switzerland, as a Postdoctoral Researcher. His main research interests include optical fiber sensing, nonlinearities in optical fiber.

Dr. Yang is a Member of the Optical Society of America.

Marcelo A. Soto received the M.Sc. degree in electronic engineering from the Universidad Técnica Federico Santa María (UTFSM), Valparaíso, Chile, in 2005, and the Ph.D. degree in telecommunications from Scuola Superiore Sant'Anna (SSSA), Pisa, Italy, in 2011.

In 2006, he was a Lecturer with the Department of Electronic Engineering, UTFSM. During 2010–2011, he was a Research Fellow at SSSA, where he was involved on distributed optical fiber sensors based on Raman and Brillouin scattering. From November 2011, he is a Postdoctoral Researcher with the Swiss Federal Institute of Technology of Lausanne, Switzerland, where he has been working on high-performance Brillouin and Rayleigh distributed fiber sensing, nonlinear fiber optics, optical signal processing, and optical Nyquist pulse generation. He is author or coauthor of about 140 scientific publications in international refereed journals and conferences in the fields of optical communications and optical fiber sensing.

Dr. Soto is a Member of the Optical Society of America, and he is in the Board of Reviewers of major international journals in photonics.

Desmond M. Chow (S'17) received the B.Eng. degree in electrical engineering and the M.Sc.Eng. degree in photonics from the University of Malaya, Malaysia, in 2011 and 2014, respectively. He is currently working toward the Ph.D. degree in photonics at the Swiss Federal Institute of Technology of Lausanne, Switzerland. His research interests include optoacoustic effect, distributed optical fiber sensors, nonlinear fiber optics, plasmonic biosensors and bandgap fibers. Mr. Chow is a Student Member of the Optical Society of America.

Pabitro Ray received the M.S. by research degree in photonics from the Indian Institute of Technology Madras, India, in 2017, and is currently working toward Ph.D. degree in photonics at the Swiss Federal Institute of Technology of Lausanne, Switzerland. His research interest includes fiber Bragg grating, distributed fiber sensing, nonlinear fiber optics, and structural health monitoring.

Luc Thévenaz (M'01–SM'12–F'17) received the M.Sc. and Ph.D. degrees in physics from the University of Geneva, Geneva, Switzerland.

In 1988, he joined the Swiss Federal Institute of Technology of Lausanne, Lausanne, Switzerland, where he currently leads a research group involved in photonics, namely fiber optics and optical sensing. Research topics include Brillouin-scattering fiber sensors, slow and fast light, nonlinear fiber optics and laser spectroscopy in gases. He achieved with his collaborators the first experimental demonstration of optically controlled slow and fast light in optical fibers, realized at ambient temperature and operating at any wavelength since based on stimulated Brillouin scattering. He also contributed to the development of Brillouin distributed fiber sensing by proposing innovative concepts pushing beyond barriers. During his career, he stayed at Stanford University, at the Korea Advanced Institute of Science and Technology, at Tel Aviv University, at the University of Sydney, and at the Polytechnic University of Valencia. In 2000, he cofounded the company Omnisens that is developing and commercializing advanced photonic instrumentation based on distributed fiber sensing.

Dr. Thévenaz is a Fellow of the Optical Society of America. He is an Associate Editor for three major scientific journals.